Projected Ranges of Energetic Ions in Solids

J.H. Liang and G.L. Kulcinski

August 1990

UWFDM-820

Published in J. Nucl. Matls. 183/3 (August 1991), pp. 202–215.

FUSION TECHNOLOGY INSTITUTE

UNIVERSITY OF WISCONSIN

MADISON WISCONSIN

Projected Ranges of Energetic Ions in Solids

J.H. Liang and G.L. Kulcinski

Fusion Technology Institute
University of Wisconsin
1500 Engineering Drive
Madison, WI 53706

http://fti.neep.wisc.edu

August 1990

UWFDM-820

Published in J. Nucl. Matls. 183/3 (August 1991), pp. 202–215.

Projected Ranges of Energetic Ions in Solids

J.H. Liang* and G.L. Kulcinski

Fusion Technology Institute
Nuclear Engineering and Engineering Physics Department
University of Wisconsin-Madison
1500 Johnson Drive
Madison WI 53706

August 1990

UWFDM-820

*current address: Advanced Nuclear Fuels Corporation, P.O. Box 130, Richland WA 99352-0130.

Abstract: Projected range equations, including nuclear and electronic losses up to the third moment, are derived as a simple and accurate means to evaluate projected ranges of energetic ions in solids. With the proposed expressions for the nuclear stopping cross section and the third-moment of both nuclear and electronic energy losses, good agreement is observed between the calculated results and experimental data for the projected ranges of ions in both single- and multi-component target materials.

1 Introduction

Ion implantation techniques have been successfully applied to improve the wear, corrosion, fatigue, and friction properties of materials, and to modify the electrical and optical properties of materials [1] in recent years. Because the properties of the implanted materials are strongly dependent on the implanted ion distribution, an accurate knowledge of the projected ranges of energetic ions in single- and even multi-component target materials is important. It is the objective of this work to derive simple and more accurate projected range equations to meet this need. Nuclear stopping cross section and third-moment of both nuclear and electronic energy losses are also derived as a reliable means to incorporate the new projected range equations. It should be noted that the present work only applies to amorphous media and crystalline effects are not included.

This paper addresses the topic in the following way. First, a brief description of models for both the nuclear and electronic energy losses is given in Section 2. Section 3 is devoted to the derivation of the new projected range equations. The calculated results and experimental data are compared and discussed in Section 4. Finally, conclusions of this work are presented in Section 5.

2 Energy loss

The slowing down of energetic ions in solids has been a subject of great theoretical and experimental interest since the early twentieth century. In gen-

eral, the nature of ion-target interaction involves all the constituents of the two interacting particles, i.e. electrons and nuclei. As suggested by Bohr [2], the energy loss of ions in a solid can be treated separately by the so-called nuclear energy loss and electronic energy loss processes. The relative importance of these two processes depends upon the instantaneous energy of the incident ion as well as the atomic number of those two interacting particles.

2.1 Nuclear energy loss

The nuclear energy loss is defined as the transfer of energy from an ion to the target atom due to an elastic collision under the influence of Coulomb fields, which are partially screened by the existing electrons. This process gives a discrete energy transfer and the amount of the energy transferred is dependent on the scattering angle during the collision. Based on the laws of energy conservation and angular momentum conservation, the scattering angle θ in the center-of-mass system between these two interacting particles can be derived as

$$\theta = \pi - 2p \int_{\infty}^{r_o} \frac{-dr}{r^2 \sqrt{1 - \frac{V(r)}{E_{co}} - \frac{p^2}{r^2}}}, \tag{1}$$

where E_{co} is the incident energy in the center-of-mass system, p is the impact parameter, r_o is the distance of the closest approach, and $V(r)$ is the interatomic potential.

In essence, $V(r)$ is represented by

$$V(r) = \frac{Z_1 Z_2 e^2}{r} \Phi(\frac{r}{a}), \tag{2}$$

where a is the characteristic screening length and Φ is the screening function. Tabulations of a and Φ can be found in the literature [3-5]. Among these expressions, the so-called universal screening function and the universal screening length [5] are adopted in this work because of their accuracy and wide acceptance. The expressions of Φ_u and a_u are respectively given by

$$\begin{aligned} \Phi_u(x) &= 0.1818e^{-3.2x} + 0.5099e^{-0.9423x} + 0.2802e^{-0.4028x} \\ &\quad + 0.02817e^{-0.2016x}, \\ a_u &= \frac{0.8854a_o}{(Z_1^{0.23} + Z_2^{0.23})}, \end{aligned} \tag{3}$$

where a_o is the Bohr radius, Z_1 and Z_2 are the atomic numbers of the incident ion and the target atom, and x is equal to r/a.

Defining the reduced energy ε and the reduced impact parameter b by the forms

$$\begin{aligned} \varepsilon &= \frac{aE_{co}}{Z_1 Z_2 e^2}, \\ b &= \frac{p}{a}, \end{aligned} \tag{4}$$

Equation 1 can be written in a more convenient expression as

$$\theta = \pi - 2b\int_0^{z_o} \frac{dz}{\sqrt{1 - \frac{z}{\varepsilon}\Phi(\frac{1}{z}) - b^2z^2}}, \tag{5}$$

where z_o is the root of the function in the denominator of Equation 5. Because there exists a singularity at $z = z_o$ in the integration term of Equation 5, it is difficult to numerically integrate Equation 5. To get around this problem, several methods have been proposed [6-9]. Among these methods, the method suggested by Everhart [6] is used in this work because of its capability of calculation for any interatomic potential. The integration term can be therefore

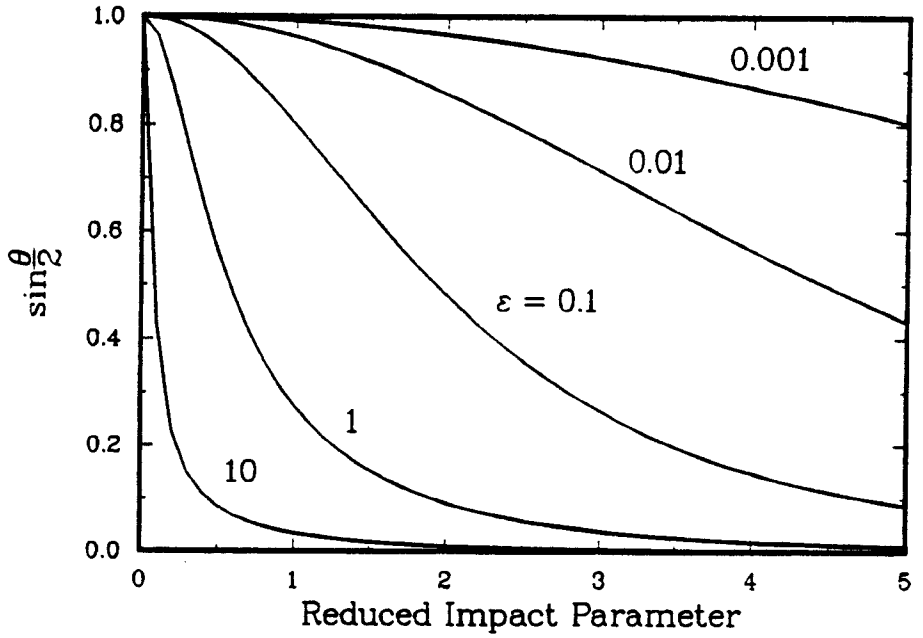

Figure 1. Scattering angle for universal potential.

rearranged as

$$I = I_1 + I_2 = \int_0^{z_o} \frac{dz}{\sqrt{1 - \frac{z}{\varepsilon}\Phi(\frac{1}{z_o}) - b^2 z^2}} + \int_0^{z_o} [\frac{1}{\sqrt{1 - \frac{z}{\varepsilon}\Phi(\frac{1}{z}) - b^2 z^2}} - \frac{1}{\sqrt{1 - \frac{z}{\varepsilon}\Phi(\frac{1}{z_o}) - b^2 z^2}}] dz, \tag{6}$$

where the first integral I_1 gives an analytic solution of

$$I_1 = \frac{1}{b}[\frac{\pi}{2} - \sin^{-1}(\frac{1 - b^2 z_o^2}{1 + b^2 z_o^2})], \tag{7}$$

and the routine D01AJF [10] based on the Gauss 10-point and Kronrod 21-point rules, is used in this work to perform numerical evaluation of the second integral I_2.

The calculated scattering angle versus reduced impact parameter for various values of reduced energy is shown in Figure 1. As can be seen, the scattering angle decreases with the increase of both the reduced energy and the reduced impact parameter.

Nuclear stopping cross section

The nuclear stopping cross section S_n, which is related to the average energy transfer T_n in a collision, is given by

$$S_n(E) = \int T_n d\sigma = \pi a^2 \Lambda E \int_0^{b^2_{max}} \sin^2 \frac{\theta}{2} d(b^2), \tag{8}$$

where Λ is the energy transfer factor $4A/(1+A)^2$ and A is the atomic mass ratio of target atom to incident ion. Using the formulation of Lindhard et al. [11], the reduced nuclear stopping s_n is defined as

$$s_n(\varepsilon) = \frac{\varepsilon}{\pi a^2 \Lambda E} S_n(E). \tag{9}$$

Following the lead of Biersack [12], the expression of the maximum impact parameter p_{max} can be simply approximated by the form [12]

$$\pi p^2_{max} = N^{-2/3}, \tag{10}$$

where N is the number density of the target material. It is recognized that the binary collision approximation will break down at extremely low energies (less than about 30 eV) [13]. However, neglecting that contribution to the range below 30 eV should have little effect.

Because of the difficulty in integrating Equation 8, many authors [14-17] have tried to evaluate the reduced nuclear stopping in an analytical way, especially with p_{max} approaching infinity. Ziegler et al. [17] approximated s_n for the universal potential by the form

$$s_n(\varepsilon) = \begin{cases} \dfrac{0.5 \ln(1+1.1383\varepsilon)}{\varepsilon + 0.01321\varepsilon^{0.21226} + 0.19593\varepsilon^{0.5}} & \varepsilon \leq 30 \\ \dfrac{0.5 \ln \varepsilon}{\varepsilon} & \varepsilon > 30. \end{cases} \tag{11}$$

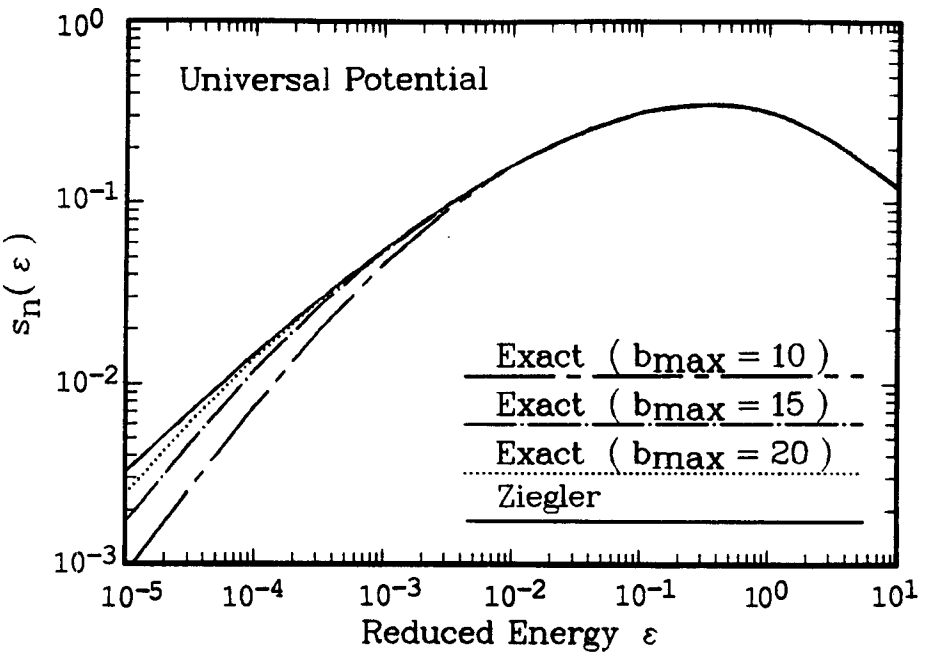

Figure 2. Reduced nuclear stopping for universal potential.

Shown in Figure 2 is a comparison of Equations 9 and 11 for the universal potential with various values of b_{max}. As can be seen, the exact solution of the reduced nuclear stopping is quite dependent on b_{max}. In general, the approximate expression shows significant deviation when the reduced energy is less than about 10^{-2} (e.g., 14 keV for bismuth in silicon or 210 eV for carbon in iron) and this deviation becomes more serious as b_{max} gets smaller. To avoid errors that may come from the analytical approximation, especially in the low energy region where the low energy heavy ion implantation or surface modification of light materials is of interest, an exact treatment of s_n for $\varepsilon < 10^{-2}$ is used in this work.

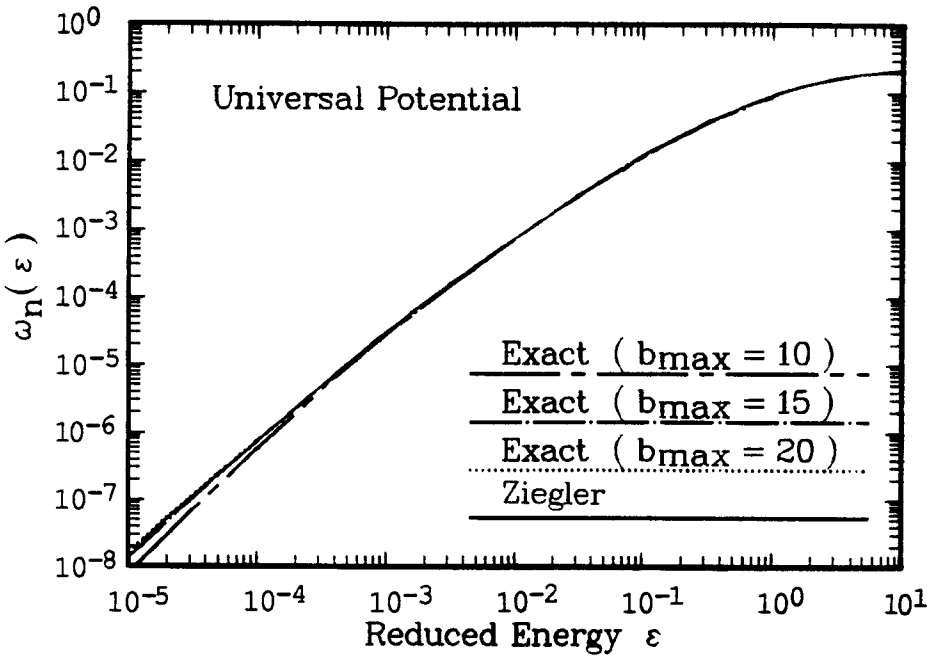

Figure 3. Reduced nuclear straggling for universal potential.

Straggling of nuclear energy loss

The straggling of nuclear energy loss, Ω_n, can be evaluated in the same way as that of the nuclear stopping cross section. That is,

$$\Omega_n(E) = \int T_n^2 d\sigma = \pi a^2 \Lambda^2 E^2 \int_0^{b^2_{max}} \sin^4 \frac{\theta}{2} d(b^2). \tag{12}$$

The reduced nuclear straggling is defined as

$$\omega_n(\varepsilon) = \frac{\varepsilon^2}{\pi a^2 \Lambda^2 E^2} \Omega_n(E). \tag{13}$$

In the analytical evaluation of ω_n for the universal potential, Ziegler et al. [17] proposed the expression

$$w_n(\varepsilon) = \frac{1}{4 + 0.197\varepsilon^{-1.6991} + 6.584\varepsilon^{-1.0494}}. \tag{14}$$

A comparison of Equations 13 and 14 for the universal potential is illustrated in Figure 3. As shown, the exact solution of the reduced nuclear

straggling exhibits only a weak dependence on the values of b_{max}, and the results of the approximate expression agree quite well with those of the exact solution. Hence, Equation 14 is used in this work because of its simplicity and savings in computer calculation time.

Third-moment of nuclear energy loss

The third-moment of nuclear energy loss, K_n, can be written as

$$K_n(E) = \int T_n^3 d\sigma = \pi a^2 \Lambda^3 E^3 \int_0^{b_{max}^2} \sin^6 \frac{\theta}{2} d(b^2), \tag{15}$$

and the reduced nuclear third-moment, κ_n, is defined as

$$\kappa_n(\varepsilon) = \frac{\varepsilon^3}{\pi a^2 \Lambda^3 E^3} K_n(E). \tag{16}$$

Because there is no approximate form of κ_n suggested, an analytical expression of κ_n is derived in this work. Based on the approximate expression of s_n given by Lindhard et al. [11], the reduced nuclear third-moment can be written as

$$\kappa_n(\varepsilon) = \frac{1}{\varepsilon^3} \int_0^{\varepsilon} (t^{1/2})^4 f(t^{1/2}) d(t^{1/2}), \tag{17}$$

where t is equal to $\varepsilon^2 \sin^2 \theta/2$ and the function $f(t^{1/2})$ is approximated by [14]

$$f(t^{1/2}) = \lambda t^{1/2-m} [1 + (2\lambda t^{1-m})^q]^{-1/q}. \tag{18}$$

To fit Equation 17 for the exact solution for the universal potential, in this work, a choice of the fitting parameters λ, m, and q is proposed to be 1.7, 0.311, and 0.588, respectively. As can be seen in Figure 4, Equation 17 shows a very good approximation to the exact solution for the universal potential. Furthermore, it can also be seen that κ_n is almost independent of b_{max}.

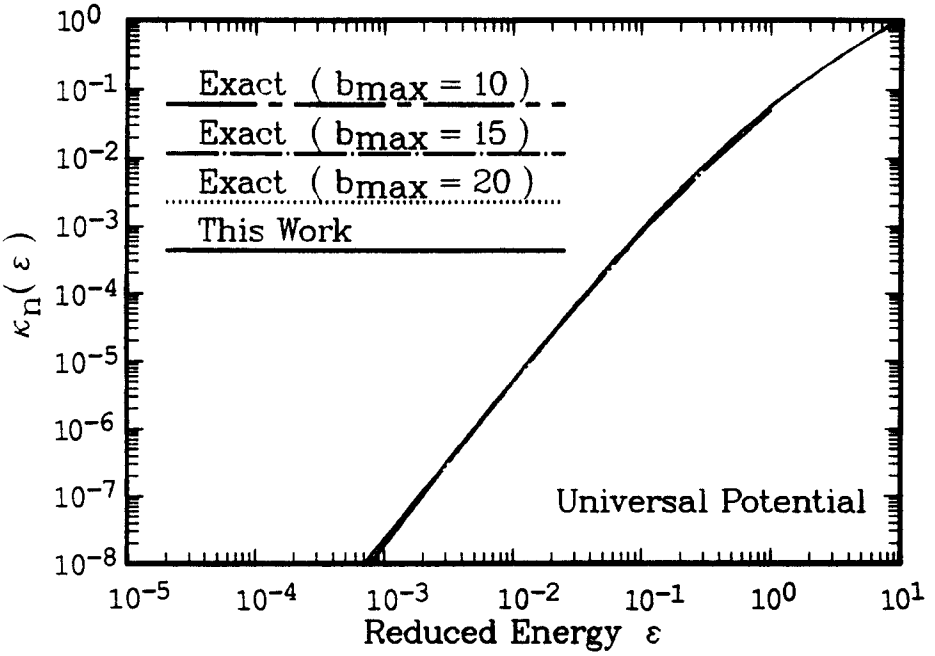

Figure 4. Reduced nuclear third-moment for universal potential.

2.2 Electronic energy loss

The electronic energy loss is defined as the energy loss of ions by excitation and ionization of the target medium. This process gives a continuous energy loss and the change of the direction of interacting particles is negligible.

Electronic stopping cross section

Based on the comparison of the velocity of ions with that of the orbital electrons in the target atoms, the electronic stopping cross section is usually divided into three energy regions: high, intermediate, and low energy. Numerous expressions of the electronic stopping cross section have been investigated theoretically and empirically. A literature survey of these investigations can be found in References [17] and [18].

With the use of both a new concept of the effective charge proposed by

Brandt and Kitagawa [19] and the local density approximation, Ziegler et al. [17] suggested a semi-empirical expression for the electronic stopping cross section S_e. In this expression, ions are basically divided into three categories according to their atomic numbers, i.e. hydrogen, helium, and heavy ions. Because the average error of this expression is proposed [17] to be only 7.8% when compared with experimental data, this expression is used in this work.

Straggling of electronic energy loss

For the straggling of electronic energy loss, Bohr [20] first suggested the expression as

$$\Omega_{e,B}(E) = \int T_e^2 d\sigma = \int_0^{2m_o v^2} T_e^2 \frac{2\pi Z_1^2 Z_2 e^4}{m_o v^2 T_e^2} dT_e, \tag{19}$$

where m_o is the electron mass. Since then, many expressions [21-24] have been proposed to improve Equation 19. Based on the free-electron-gas model, Bonderup and Hvelplund [24] suggested an analytical expression of the form

$$\frac{\Omega_e}{\Omega_{e,B}} = \begin{cases} 1 + [0.2(\frac{v_F}{v})^2 + \frac{\hbar\omega_o}{2m_o v^2}] \ln(\frac{v}{v_F})^2 & v >> v_F \\ (1 + 13\chi^2)^{-0.5} (\frac{v}{v_F})^2 & v \leq v_F, \end{cases} \tag{20}$$

where χ^2 is equal to $e^2/\pi\hbar v_F$, while v_F and ω_o are the Fermi velocity and the plasma frequency of the target material, respectively. Equation 20 is used in this work. The expression of $\Omega_{e,B}$ will include the relativistic effect [21], and is given by

$$\Omega_{e,B} = 4\pi Z_1^2 Z_2 e^4 (\frac{1 - 0.5\beta^2}{1 - \beta^2}), \tag{21}$$

where β is equal to v/c and c is the speed of light.

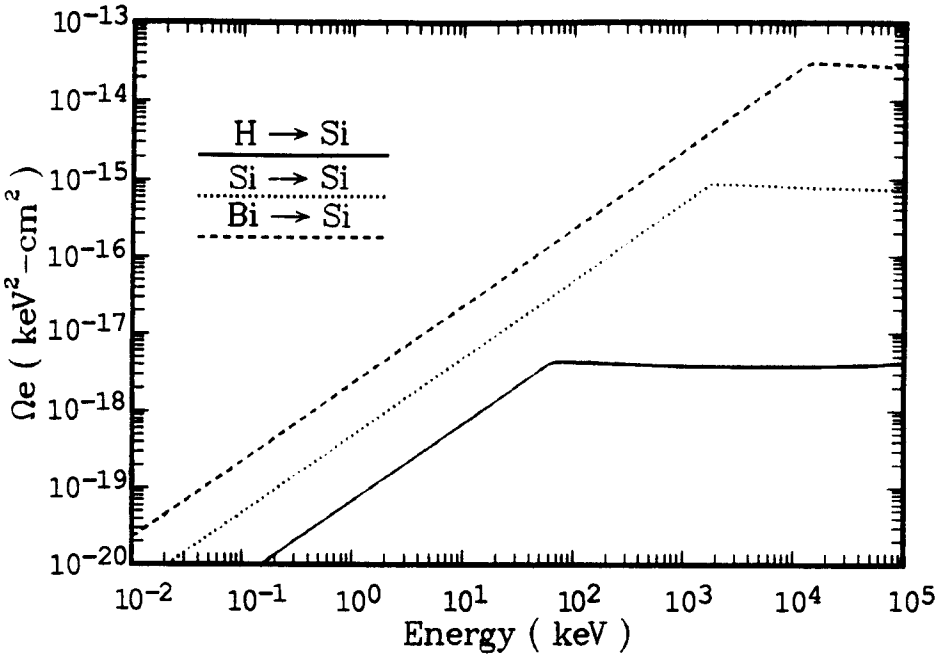

Figure 5. Straggling of electronic energy loss for H, Si, and Bi in Si.

A representation of the straggling of electronic energy loss for hydrogen, silicon, and bismuth ions in silicon is displayed in Figure 5. As can be seen, the heavier ion shows a larger straggling of electronic loss. In addition, the straggling of electronic energy loss increases roughly proportionally to the ion energy, especially at low energies, and approaches a constant as the ion velocity becomes much greater than the Fermi velocity.

Third-moment of electronic energy loss

As present, there is no proposed analytical expression for the third-moment of electronic energy loss, K_e. The following equation, similar to Bohr's theory, is therefore derived in this work:

$$K_e(E) = \int T_e^3 d\sigma = \int_0^{2m_o v^2} T_e^3 \frac{2\pi Z_1^2 e^4}{m_o v^2 T_e^2} dT_e. \tag{22}$$

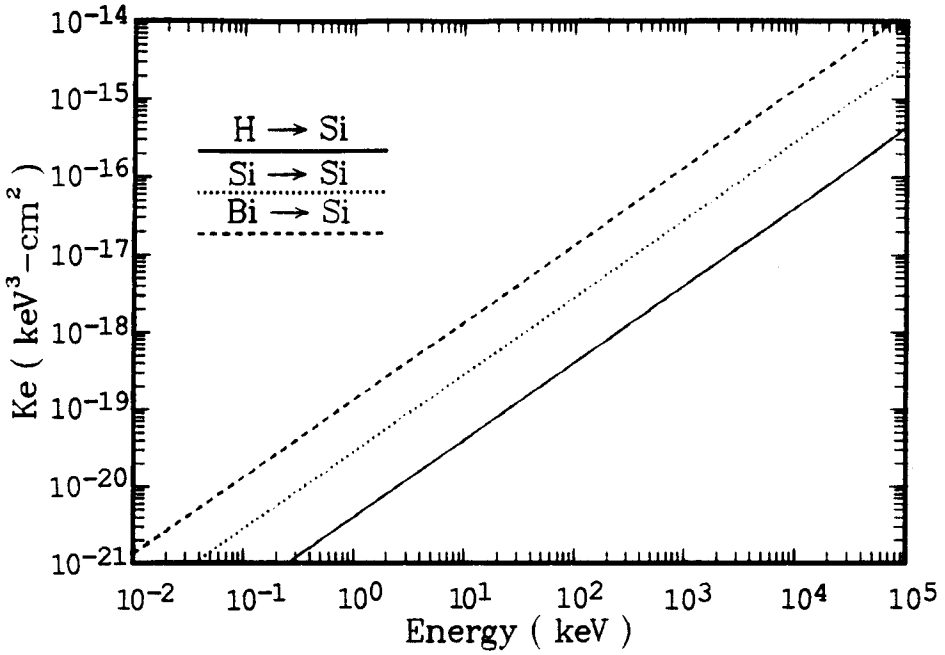

Figure 6. Third-moment of electronic energy loss for H, Si, and Bi in Si.

To account for the relativistic effect, Equation 22 can be further written in the form of

$$K_e(E) = 8\pi Z_2 Z_1^2 e^4 m_o v^2 \left(\frac{1/2 - \beta^2/3}{1 - \beta^2}\right). \tag{23}$$

Plotted in Figure 6 is a demonstration of the third-moment of electronic energy loss for hydrogen, silicon, and bismuth ions in silicon. As shown, the heavier ion represents a larger value of the third-moment of electronic energy loss. The third-moment of electronic energy loss also shows a linear increase with the ion energy.

3 Projected range formulation

In this work, the projected range formulation is derived on the basis of the backward type linearized Boltzmann equation in which the governing equation

is given by [25]

$$n\overline{x^{n-1}z^m} = N\int d\sigma \overline{x^n z^m} - N\int d\sigma \int\int\int dx^* dy^* dz^* \qquad (24)$$
$$(x^*\cos\phi - z^*\sin\phi)^n (x^*\sin\phi + z^*\cos\phi)^m p_o(E-T, x^*, y^*, z^*),$$

where $T = T_n + T_e$, x is the coordinate along with the original direction of the incident ions, and z is the lateral coordinate relative to x. The deflection angle ϕ is given by

$$\begin{aligned} \tan\phi &= \frac{\sin\theta}{\cos\theta + 1/A}, \qquad (25) \\ \sin\frac{\theta}{2} &= (1+A)\sqrt{\frac{T_n}{4AE}}. \end{aligned}$$

The spatial moments of the projected range distribution p_o are defined as

$$\overline{x^n z^m} = \int\int\int x^{*n} z^{*m} p_o(E, x^*, y^*, z^*) dx^* dy^* dz^*. \qquad (26)$$

To solve Equation 24, Biersack [25] used a Taylor series expansion of p_o, $\cos\phi$, and $\sin\phi$ up to the second moment. This procedure is extended to the third moment in this work and the projected range equations can be derived as the following third-order coupled differential equations:

$$\begin{aligned} NS \quad & \{(\frac{K}{6S})\frac{d^3\overline{x^2}}{dE^3} + (\frac{\Omega}{2S} + \frac{AK_n}{4ES})\frac{d^2\overline{x^2}}{dE^2} \qquad (27) \\ & + [1 + \frac{A\Omega_n}{2ES} + \frac{(1-2A)K_n}{8E^2S}]\frac{d\overline{x}}{dE}\} \\ & = 1 - N[\frac{AS_n}{2E} - \frac{(1-2A)\Omega_n}{8E^2} - \frac{(2-3A)K_n}{16E^3}]\overline{x}, \end{aligned}$$

$$\begin{aligned} NS \quad & [\frac{d(\overline{x^2}+\overline{z^2})}{dE} - \frac{\Omega}{2S}\frac{d^2(\overline{x^2}+\overline{z^2})}{dE^2} + \frac{K}{6S}\frac{d^3(\overline{x^2}+\overline{z^2})}{dE^3}] \\ & = 2\overline{x}, \end{aligned}$$

$$
\begin{aligned}
NS \quad & [\frac{d\overline{z^2}}{dE} - \frac{\Omega}{2S}\frac{d^2\overline{z^2}}{dE^2} + \frac{K}{6S}\frac{d^3\overline{z^2}}{dE^3}] \\
& = N\{[\frac{AS_n}{E} - \frac{(1-A)^2\Omega_n}{4E^2} - \frac{(1-A)^2K_n}{4E^3}](\overline{x^2} - \overline{z^2}) \\
& \quad -[\frac{A\Omega_n}{E} - \frac{(1-A)^2K_n}{4E^2}]\frac{d}{dE}(\overline{x^2} - \overline{z^2}) \\
& \quad -\frac{AK_n}{2E}\frac{d^2}{dE^2}(\overline{x^2} - \overline{z^2})\,\}.
\end{aligned}
$$

As suggested by Biersack [25], the second and third derivative terms, d^2/dE^2 and d^3/dE^3, in Equation 27 can be simply reduced into first derivatives of E, d/dE, by using the approximations of

$$
\begin{aligned}
\overline{x} &\propto E^{1/2}, \\
\overline{x^2} &\propto E, \\
\overline{z^2} &\propto E,
\end{aligned}
\tag{28}
$$

where $\overline{x}$ is the projected range, $(\overline{x^2} - \overline{x}^2)^{1/2}$ represents the projected range straggling, and $(\overline{z^2})^{1/2}$ denotes the projected range lateral straggling. With these simplifications, Equation 27 can be expressed as the following first-order coupled differential equations:

$$
\begin{aligned}
NS \quad & [1 + \frac{\Omega - 2A\Omega_n}{4ES} + \frac{K + (1-3A)K_n}{8E^2S}]\frac{d\overline{x}}{dE} \\
& = 1 - N[\frac{AS_n}{2E} - \frac{(1-2A)\Omega_n}{8E^2} - \frac{(2-3A)K_n}{16E^3}]\overline{x},
\end{aligned}
\tag{29}
$$

$$
NS \quad \frac{d(\overline{x^2} + \overline{z^2})}{dE} = 2\overline{x},
$$

$$NS \quad [1 - \frac{2A\Omega_n}{ES} + \frac{(1-A)^2 K_n}{2E^2 S}] \frac{d\overline{z^2}}{dE}$$
$$= N[\frac{AS_n}{E} - \frac{(1-A)^2\Omega_n}{4E^2} - \frac{(1-A)^2 K_n}{4E^3}](\overline{x^2} - \overline{z^2})$$
$$-[\frac{2A\Omega_n}{ES} - \frac{(1-A)^2 K_n}{2E^2 S}]\overline{x},$$

where $S = S_n + S_e$ and with similar expressions for Ω and K. Due to the fact that the term $[1 - 2A\Omega_n/ES + (1-A)^2 K_n/2E^2 S]$ can be zero for some ion-target combinations, a further investigation of Equations 28 and 29 is needed. With the use of $\overline{z^2} \propto E$ in approximating the term $[-2A\Omega_n/ES + (1-A)^2 K_n/2E^2 S]\ d\overline{z^2}/dE$, the projected range equations for any ion-target combination can be obtained as

$$NS \quad [1 + \frac{\Omega - 2A\Omega_n}{4ES} + \frac{K + (1-3A)K_n}{8E^2 S}] \frac{d\overline{x}}{dE} \tag{30}$$
$$= 1 - N[\frac{AS_n}{2E} - \frac{(1-2A)\Omega_n}{8E^2} - \frac{(2-3A)K_n}{16E^3}]\overline{x},$$

$$NS \quad \frac{d(\overline{x^2} + \overline{z^2})}{dE} = 2\overline{x},$$

$$NS \quad \frac{d\overline{z^2}}{dE} = N[\frac{AS_n}{E} - \frac{(1-A)^2\Omega_n}{4E^2} - \frac{(1-A)^2 K_n}{4E^3}](\overline{x^2} - \overline{z^2})$$
$$-[\frac{2A\Omega_n}{ES} - \frac{(1-A)^2 K_n}{2E^2 S}](\overline{x} - NS\frac{\overline{z^2}}{E}).$$

To extend the application of Equation 30 for multi-component target materials, the so-called Bragg rule [26] is used. In Bragg's formulation, the electronic stopping cross section of a $B_m C_n$ material is simply expressed as

$$S_e(B_m C_n) = mS_e(B) + nS_e(C), \tag{31}$$

where $S_e(B)$ and $S_e(C)$ are the electronic stopping cross sections of the components B and C, respectively. Define the following:

$$\begin{aligned} A^i S_e &= \sum_j A_j^i f_j S_{ej}, \\ A^i \Omega_e &= \sum_j A_j^i f_j \Omega_{ej}, \\ A^i K_e &= \sum_j A_j^i f_j K_{ej}, \end{aligned} \tag{32}$$

where the exponent $i = 0, 1$, and 2, f_j is the atomic fraction of the j^{th} component in the target material, and A_j is equal to the atomic mass ratio of the j^{th} component to incident ion. An expression similar to that of Equation 32 is used for the nuclear energy loss.

4 Results and discussion

In Figure 7, the calculated projected range R_p and range straggling ΔR_p for heavy ions such as bismuth in silicon are depicted as functions of energy. The experimental data [27-30] and the theoretical data from the well-known Monte Carlo computer code TRIM [31] are also shown. As can be seen, this work as well as TRIM show good agreement with experimental data at low energies, but this work shows superior agreement at high energies.

Shown in Figures 8 and 9 are the comparisons of the calculated results from this work with experimental data [32-38] for the projected range and range straggling of medium ions such as boron and phosphorous in silicon. The good agreement is obvious. For the implantation of light ions such as helium and hydrogen in silicon, an inspection of Figures 10 and 11 shows that the calculated results also compare well with experimental data [39-44].

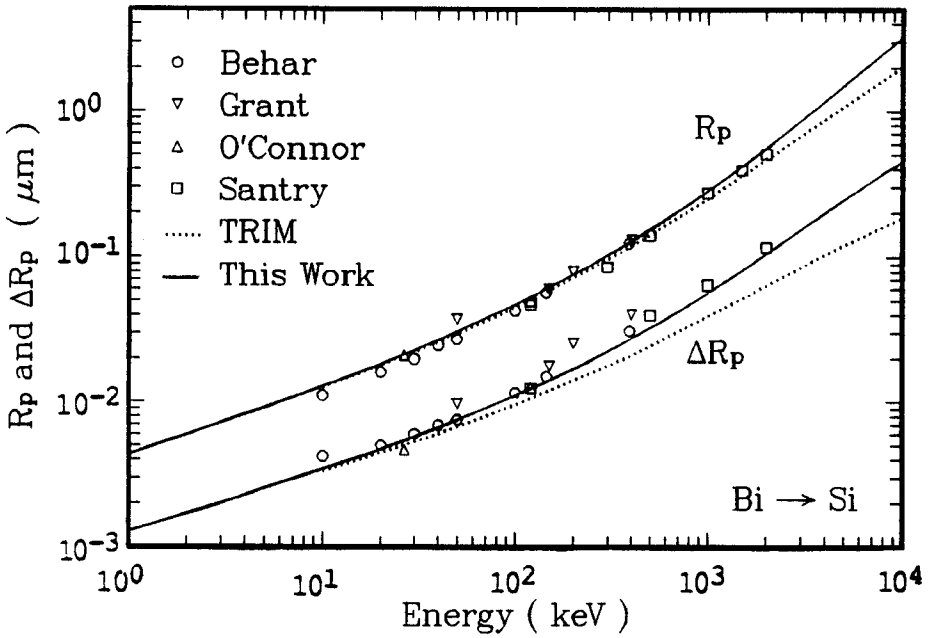

Figure 7. Projected range and range straggling of Bi in Si.

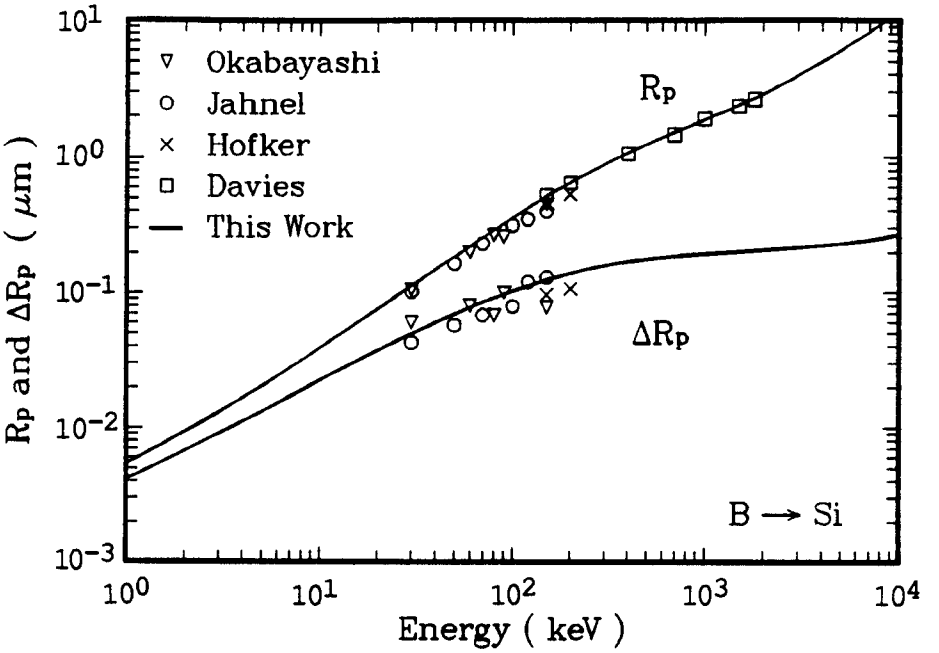

Figure 8. Projected range and range straggling of B in Si.

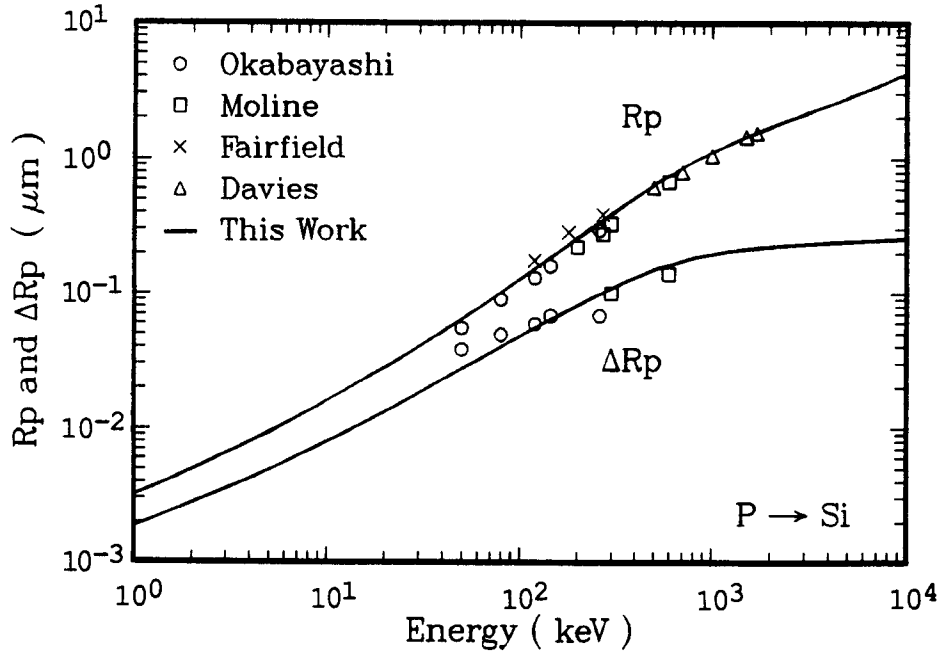

Figure 9. Projected range and range straggling of P in Si.

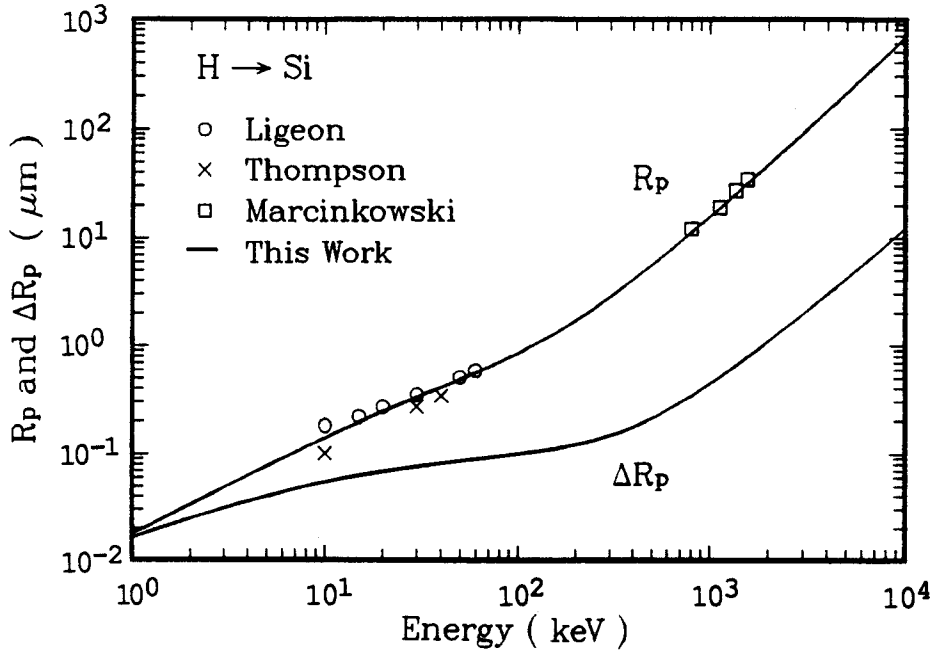

Figure 10. Projected range and range straggling of He in Si.

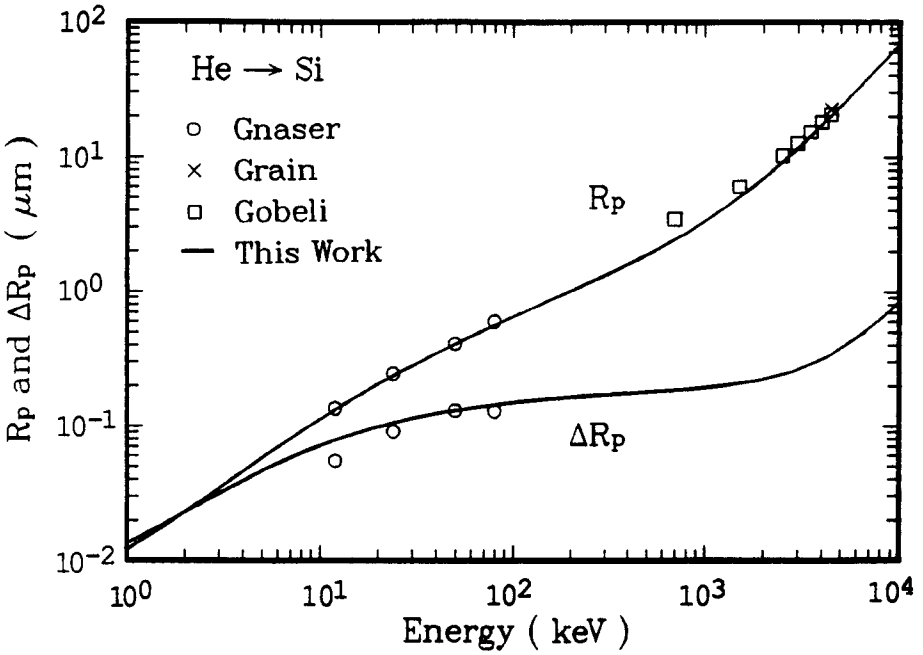

Figure 11. Projected range and range straggling of H in Si.

In addition, the calculated lateral straggling $\Delta R_{\perp}$ for lead ions in silicon is displayed along with experimental data [29] in Figure 12. As can be seen, the calculated results agree very well with experimental data. A comparison of the calculated results with experimental data for a compound substrate such as silicon dioxide [45] has also been investigated. From Figures 13 and 14, it can again be seen that the agreement is quite good.

5 Conclusions

It has been found that the use of the recently-derived projected range equations, together with the nuclear and electronic energy losses up to the third moment, leads to a simple and accurate means of evaluating the projected ranges of energetic ions in either single-component target materials or

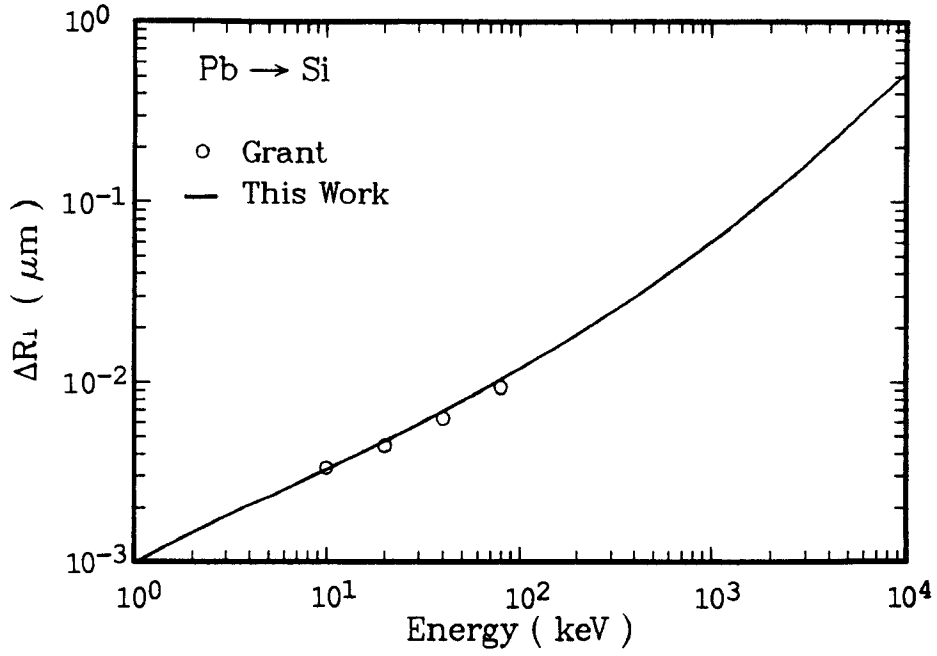

Figure 12. Projected range lateral straggling of Pb in Si.

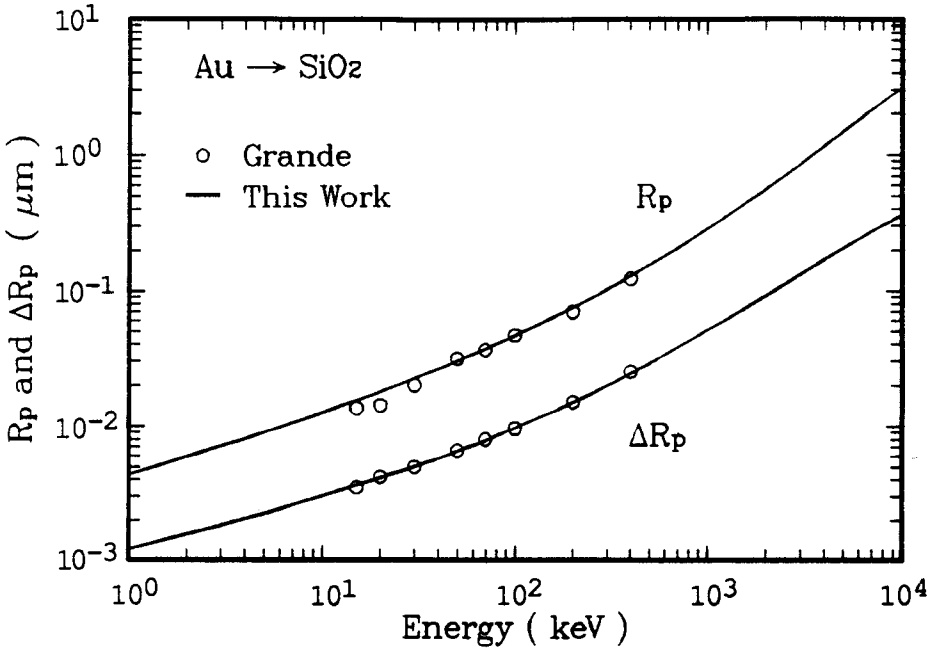

Figure 13. Projected range and range straggling of Bi in SiO_2.

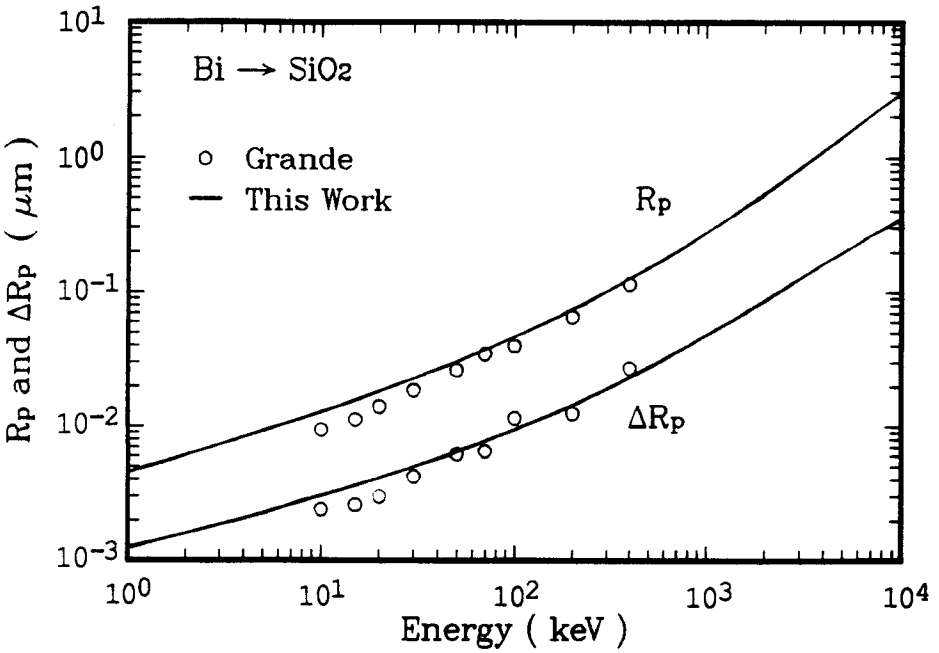

Figure 14: Projected range and range straggling of Au in SiO_2.

multi-component target materials such as chemical compounds, alloys, mixtures, etc. In addition, it should be noted that the good correlation between this work and experiment is obtained without resorting to any empirical correction factors.

Acknowledgments

This work was supported by the United States Department of Energy. The authors wish to thank Prof. J. P. Blanchard for numerous enlightening discussions.

References

[1] J. R. Conrad et al., J. Appl. Phys. 62 (1987) 4591.

[2] N. Bohr, Phil. Mag. 25 (1913) 10.

[3] I. M. Torrens, "Interatomic Potentials," Academic Press, New York (1972).

[4] W. D. Wilson, L. G. Haggmark, and J. P. Biersack, Phys. Rev. 15B (1977) 58.

[5] J. P. Biersack and Z. F. Ziegler, Springer Series in Electrophysics 10 (1982) 122.

[6] E. Everhart, G. Stone, and R. J. Carbone, Phys. Rev. 99 (1955) 1287.

[7] F. J. Smith, Physica 30 (1964) 497.

[8] F. J. Smith and R. J. Munn, J. Chem. Phys. 41 (1964) 3560.

[9] M. Kennedy and F. J. Smith, Mol. Phys. 13 (1967) 443.

[10] NAG Fortran Library Manual, Mark 11, Volume 1, Numerical Algorithms Group, Oxford, United Kingdom (1984).

[11] J. Lindhard, V. Nielsen, and M. Scharff, Mat. Fys. Medd. Dan. Vid. Selsk. 36, No. 10 (1968).

[12] J. P. Biersack and L. G. Haggmark, Nucl. Instr. and Meth. 174 (1980) 257.

[13] M. T. Robinson and I. M. Torrens, Phys. Rev. B9 (1974) 5008.

[14] K. B. Winterbon, Rad. Eff. 13 (1972) 215.

[15] I. Adesida and L. Karapiperis, Rad. Eff. 61 (1982) 223.

[16] O. S. Oen and M. T. Robinson, J. Appl. Phys. 46 (1975) 5069.

[17] Z. F. Ziegler, J. P. Biersack, and U. Littmark, "Stopping and Range of Ions in Solids," Volume 1, Pergamon Press, New York (1985).

[18] M. A. Kumakhov and F. F. Komarov, "Energy Loss and Ion Ranges in Solids," translated from the Russian by B. Teague, Gordon and Breach Science Publishers Inc., New York (1981).

[19] W. Brandt and M. Kitagawa, Phys. Rev. B25 (1982) 5631.

[20] N. Bohr, Mat. Fys. Medd. Dan. Vid. Selsk. 18, No. 8 (1948).

[21] D. Pines and D. Bohm, Phys. Rev. 85 (1952) 338.

[22] M. S. Livingston and H. A. Bethe, Rev. Mod. Phys. 9 (1937) 245.

[23] J. Lindhard and M. Scharff, Mat. Fys. Medd. Dan. Vid. Selsk. 27, No. 15 (1953).

[24] E. Bonderup and P. Hvelplund, Phys. Rev. A4 (1971) 562.

[25] J. P. Biersack, Z. Physik A (Atoms and Nuclei), 95 (1982) 305.

[26] W. H. Bragg and R. Kleeman, Philos. Mag. 10 (1905) 318.

[27] M. Behar et al., Nucl. Instr. and Meth. B6 (1985) 453.

[28] D. J. O'Connor, Nucl. Instr. and Meth. 196 (1982) 493.

[29] W. A. Grant, J. S. Williams, and D. Dodds, "Measurement of Projected and Lateral Range Parameters for Low Energy Heavy Ions in Silicon by Rutherford Backscattering," Proc. 2nd Int. Conf. on Ion Beam Layer

Analysis, Karlsruhe, edited by O. Meyer et al., Plenum Press, New York (1976) p.235.

[30] D. C. Santry and R. D. Werner, Nucl. Instr. and Meth. 139 (1976) 135.

[31] J. F. Ziegler "TRIM-89 The TRansport of Ions in Matter, Version 5.4," International Business Machines Corp., New York (1989).

[32] H. Okabayashi and D. Shinoda, J. Appl. Phys. 44 (1973) 4220.

[33] H. Okabayashi and D. Shinoda, Japan J. Appl. Phys. 13 (1974) 1187.

[34] R. A. Moline, J. Appl. Phys. 42 (1971) 3553.

[35] J. M. Fairfield and B. L. Crowder, Trans. AIME 245 (1969) 469.

[36] F. Jahnel et al., Nucl. Instr. and Meth. 182/183 (1981) 223.

[37] W. K. Hofker et al., Rad. Eff. 24 (1975) 223.

[38] D. E. Davies, Can. J. Phys. 47 (1969) 1750.

[39] H. Gnaser et al., Nucl. Instr. and Meth. B15 (1986) 49.

[40] A. Grain and H. Faraggi, J. Phys. Radium 19 (1958) 76.

[41] G. W. Gobeli, Phys. Rev. 103 (1956) 275.

[42] E. Ligeon and A. Guivarc'h, Rad. Eff. 27 (1976) 129.

[43] D. A. Thompson and J. E. Robinson, Nucl. Instr. and Meth. 132 (1976) 261.

[44] A. Marcinkowski, H. Rzewuski, and Z. Werner, Nucl. Instr. and Meth. 57 (1967) 338.

[45] P. L. Grande et al., Nucl. Instr. and Meth. B19/20 (1987) 25.